

North sea produced water PAH exposure and uptake in early life stages of Atlantic Cod

Raymond Nepstad*, Bjørn Henrik Hansen, Jørgen Skancke

SINTEF Ocean, Trondheim, Norway

ABSTRACT

Produced water discharges from offshore oil and gas platforms represent a significant source of petroleum components such as polycyclic aromatic hydrocarbons (PAHs) released to the ocean. High molecular weight PAHs are persistent in the environment and have a potential for bioaccumulation, and the investigation of their fate and uptake pathways in marine life are relevant when assessing environmental risk of produced water discharges. To study the exposure and uptake of 2–5 ring PAHs in early life stages of Atlantic Cod in the North Sea, we run a coupled fate and individual-based numerical model that includes discharges from 26 platforms. We consider 26 different PAH components in produced water which biodegrade with primary degradation rates; intermediate degradation products are not included. Model simulations are run covering multiple years (2009–2012) to study annual exposure variability, while a one-day time slice of spawning products from the peak spawning season are followed. By covering multiple release points and large spatio-temporal scales, we show how individuals can be exposed to produced water from multiple regions in the North Sea. We find that a combination of oceanic fate processes and toxicokinetics lead to markedly different compositions in the predicted internal concentrations of PAHs compared to discharge concentrations; for instance, naphthalene makes up 30% of the total discharged PAHs, but contributes to at most 1% of internal concentrations. In all simulations we find the predicted total internal PAH concentration (26 components) to be below 1.2 nmol/g, a factor of 1000 less than concentrations commonly associated with acute narcotic effects.

1. Introduction

Produced water (PW) discharges from offshore oil and gas production represent the largest discharge to the marine environment worldwide, with approximately 1.3×10^8 m³ released annually on the Norwegian continental shelf (NCS). PW contains a mixture of formation water, oil, gas, injected fresh/brine water and added production chemicals. The formation water contains a mixture of dissolved inorganic and organic components, and the composition varies between different reservoirs (Neff et al., 2011). Total PW discharges from activities on the NCS in 2017 included 129 tons polycyclic aromatic hydrocarbons (PAHs) (NOROG, 2018). Despite being a small fraction (0.306%) of the total composition of produced water, PAHs are considered a key risk component (Beyer et al., 2020). These PAHs can be dissolved in the water, present in dispersed oil droplets and/or adsorbed to particulates (Faksness et al., 2004). Different PAHs display varying lifetimes and biological uptake properties in the ocean. In general biodegradation rates tend to decrease with increasing molecular weight of PAHs (Lofthus et al., 2018), and the potential for bioaccumulation (bioconcentration) tend to increase with molecular weight (De Hoop et al., 2013).

The Atlantic cod (*Gadus morhua*) is found throughout the Northern Atlantic Ocean where it has been one of the most commercially important species for centuries (Otterå, 2004). Cod populations in the North Sea have declined (Brander, 2005), and it is labelled vulnerable

on the IUCN Red List of Threatened species. Apart from overfishing, recruitment failure is generally believed to be a main contributor to the decline, the causes of which are complex (Huserbråten et al., 2018; Akimova et al., 2019). Important spawning grounds for Atlantic cod in the North and Norwegian Seas are found in vicinity of oil production fields with produced water discharges (see Fig. 1 and Akimova et al., 2019; Sundby et al., 2017). The spawning season for cod in North Sea extends from January to May, with a peak in February and March (Sundby et al., 2017), and the eggs develop over a period of approximately 100 degree-days before hatching (Fraser et al., 1988). After fertilization, eggs are positively buoyant in seawater and are therefore found in the upper water masses. After hatching the larvae drift with ocean currents and perform vertical migration (Vikebø et al., 2007).

Exposure of early developmental life stages (ELS) to petrogenic compounds has shown to cause acute toxicity as well as a range of sub-lethal effects. Atlantic cod and Atlantic haddock (*Melanogrammus aeglefinus*) embryos exposed to oil dispersions showed craniofacial deformations in hatched larvae. This occurred for exposure concentrations above 0.76 (haddock) and 2.8 (cod) µg TPAH/L, and associated with TPAH internal concentrations of 542 ng/g (wet weight) for cod (Sørensen et al., 2017). In another study, cardiotoxicity and severe craniofacial deformations were observed in cod larvae after embryonic exposure to PW extracts corresponding to 50–500-fold dilutions of PW (ranging 2.5–34 µg TPAH/L) (Hansen et al., 2019). These studies have only measured

* Corresponding author.

E-mail address: raymond.nepstad@sintef.no (R. Nepstad).

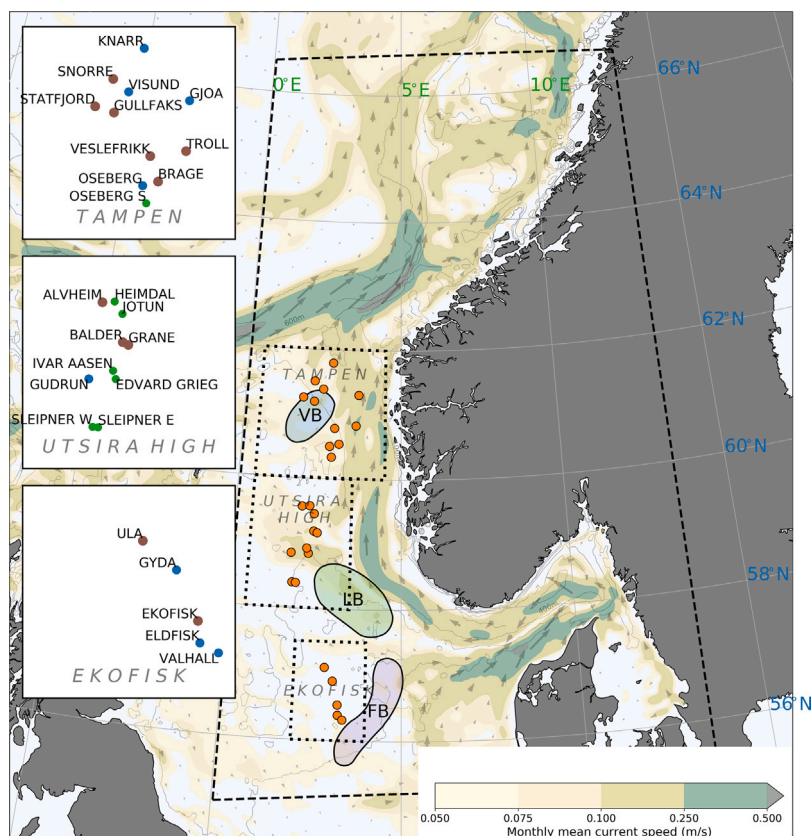


Fig. 1. Study area and model domain (dashed line), with each produced water source marked as orange circles. The insets show the names of each discharge point in the three regions, outlined by the dotted black lines (Tampen, Utsira High and Ekofisk), with colours indicating the yearly amount of PAHs discharged (dark red: > 1000 kg, blue: 100–1000 kg, green: < 100 kg). The coloured polygons indicate the spawning grounds used in the simulations (Blue — Viking Bank, Green — Ling Bank and Purple — Fisher Bank). Monthly mean ocean currents for March 2009 are also shown. The black dashed line is the outline of the main computational domain. (For interpretation of the references to colour in this figure legend, the reader is referred to the web version of this article.)

a sub-set of components (PAHs and alkylated homologues) present in the oil dispersions and PW, and the contribution of non-quantified components to toxicity has not been determined. Studies with single PAH components have also shown embryotoxicity; a study with phenanthrene exposure (45–85 $\mu\text{g/L}$) resulted in severe deformations, with body residues in the range of 20–30 $\mu\text{g/g}$ (wet weight) (Sørensen et al., 2019).

In this study, the DREAM model (Reed and Hetland, 2002; Reed and Rye, 2011) was used to evaluate the potential for bioaccumulation of PAHs from PW in cod populations ELS. DREAM is routinely used to predict the physical transport and fate of produced water, and in risk assessment by calculating ratio of predicted environmental concentration (PEC) and predicted no effect concentration (PNEC) of individual PW substances (see e.g. Smit et al., 2011; Beyer et al., 2012). Several studies have also compared predictions from the model with field measurement (Durell et al., 2006; Niu et al., 2016).

Given the temporal and spatial distribution of concentrations in a PW plume, impact on marine life can be assessed through coupling with individual-based models (IBM) (Grimm and Railsback, 2005; Scheffer et al., 1995) and toxicokinetic models (McCarty and Mackay, 1993; Hendriks et al., 2001; Jager et al., 2011). Whereas the individual-based models are used to model the behaviour of population individuals or groups of these, toxicokinetic models are used to predict internal concentrations given the external concentration of components in the PW plume. The resulting internal concentrations, also known as body residues or body burdens, are more closely related to the effective dose than the environmental exposure concentrations, and are thus more relevant for predicting effects and environmental risks (Meador et al., 2008; Ashauer and Escher, 2010; Jager et al., 2011). Internal concentrations can also be determined for oceanic organisms sampled

in the field (see e.g. Durell et al., 2006; Hansen et al., 2020), which may potentially be useful for comparison with model predictions.

2. Materials and method

2.1. Study area and produced water discharge data

PW discharge concentration profiles containing 26 different PAH components from 26 distinct offshore platforms in the North Sea were used as input to the simulations (Fig. 1). A list of the individual PAH components and their relevant physico-chemical properties, concentrations in the discharge, and details on each release site are given in the Supplementary Information. Site-specific release rates, varying from 3000–66 000 m^3/day , and composition profiles for each platform are shown in Fig. 2. These were obtained from the Norwegian Environment Agency based on annual reports from oil and gas operators (see e.g. Equinor, 2018). Release rates represent a yearly average rate, and the depths of the discharges vary from 1 to 40 m. The geographic positions of the offshore platforms are based on data from the Norwegian Petroleum Directorate fact pages.¹ An overview of the study area, showing release sites and spawning grounds, is shown in Fig. 1 where the release sources have been grouped within three different regions marked: Tampen, Utsira High and Ekofisk. The named component groups used in the figure are naphthalenes (naphthalene and C1–C3 alkyl homologs), phenanthrenes (phenanthrene and C1–C3 alkyl homologs) and dibenzothiophenes (dibenzothiophene and C1–C3 alkyl homologs), while the remaining 14 components are included in

¹ <https://factpages.npd.no/>

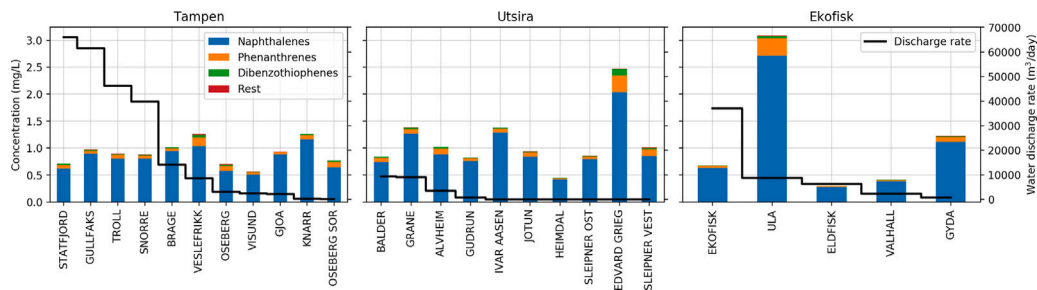


Fig. 2. An overview of the produced water discharges used in the simulation, showing the discharge concentrations of component groups (bars) and total water discharge rates (black line) for each point source, grouped by region.

the “Rest” category. The three named groups constitute the majority of the PAHs in the discharge, and are the most relevant for analysing internal concentrations. In the discussion of simulation results, the full 26 components are referred to as total PAH, in the sense of total PAH in the simulated discharge. A complete list of names and properties of the PAHs included in the simulations is given in Table 2 in the Supplementary Information.

2.2. Ocean circulation data

Simulating advective transport of contaminants and biological individuals require an external circulation field. To investigate the potential variation in exposure in different years, we used an archive of ocean circulation model data covering the model domain over four years (2009–2012), with a horizontal resolution of 4 km. Monthly mean surface currents from the archive for March 2009 are shown in Fig. 1. This archive was produced with the hydrodynamic component of the SINMOD model system, which is based on the primitive Navier–Stokes equations (Slagstad and McClimans, 2005). SINMOD uses a z-coordinate grid, and in the present archive uses 33 vertical levels, with layer thicknesses ranging from 5 m in the upper layers (down to 40 m depth), increasing to 50 m in the intermediate layers (100 m–1000 m depth), then to 500 m in deeper layers (below 1000 m depth) (Alver et al., 2016).

2.3. Produced water transport and fate

Transport of produced water in DREAM is handled by a Lagrangian particle approach (DREAM, Reed and Hetland, 2002; Reed and Rye, 2011) which tracks each discharge component in the receiving environment. The produced water release does not include dispersed oil droplets, treating the discharge as a release of purely dissolved compounds. Eulerian concentration grids are calculated from the mass and distribution of the particles which provides the input to the exposure model. Two resolution levels of grids are used: near the discharge sources 1 km x 1 km cell size grids are used for improved resolution, corresponding approximately to the regional outlines (dotted lines) in Fig. 1, while the whole computational domain (dashed outline in Fig. 1) is covered by a second, coarser grid (4 km x 4 km). To cover the peak spawning season in the North Sea the model was run for the months of March, April and May for each of the years from 2009 to 2012.

In addition to advection and turbulent diffusion, the model calculates bacterial degradation of PAHs based on first-order kinetics and primary biodegradation reference rates (Lofthus et al., 2018) given in Table 5 in the Supplementary Information. By using primary degradation rates we track fate of the original PW components in the water column, and do not follow further degradation products. Each PW component is associated with a specific biodegradation rate. For the component groups that have been used, half lives vary from a few days for the low molecular weight components to over a year for the heaviest components. Water temperature affects the biodegradation

rates, which is accounted for by scaling the rates according to the Q10-approach (Bagi et al., 2013), using the temperature at the location of each Lagrangian particle. In the present simulations, a constant sea water temperature of 10 °C was used. A constant temperature was selected to focus the analysis on the variation of ocean currents between the chosen months and years in the study. The temperature of 10 °C is in the high end but within observed values for March, April and May in the North Sea. Another fate outcome for produced water is evaporation through the sea surface. Evaporation is included by default in DREAM, but contributes to a negligible fraction of produced water’s mass balance.

To represent the produced water discharges in the simulations a maximum total number of 70 000 particles was used, with 10 particles being released from each discharge site in each time step, and the main model time step was 15 set to minutes. Sub-grid transport and mixing not resolved by the ocean model are typically accounted for by adding a horizontal diffusivity in the particle model. The value of this parameter depends on the resolution of the ocean model, with higher values typically used for coarser models. Different values have been reported in recent model studies: 10 m²/s was used in studies of the Deep Water Horizon oil spill (Boufadel et al., 2014; Berenshtein et al., 2020), while Simonsen et al. (2017) experimented with different horizontal diffusivity values (0 and 100 m²/s) in a 4 km ocean model setup in a study of radionuclide tracer transport in the North Sea and found that it had only minor impacts on model skill. In the present study we used a fixed horizontal diffusivity value of 50 m²/s, which is comparable to median values calculated on the ocean model flow field with the Smagorinsky method, which accounts for resolution and shear in the mean flow field (Smagorinsky, 1963). A sensitivity test was also performed on this value, which is given in the Supplementary Information.

The vertical diffusivity was set to a constant value 10⁻⁴ m²/s, which corresponds to low vertical mixing conditions. Higher values of vertical diffusivity, caused by e.g. strong winds, can occur near the surface, and would lead to increased dilution and lower concentrations. Deeper in the water column lower diffusivity values are generally expected, with a large seasonal variation in the surface mixed layer in the North Sea. Uniform values have been used in previous model studies, such as Paris et al. (2012), where the Macondo oil well blowout was modelled using a fixed diffusivity value of 10⁻⁵ m²/s, although focusing on deeper waters than here (around 1000 m). Differences between uniform and depth-varying profiles of vertical diffusivities have been explored by several authors, for some recent in-depth discussions see e.g. Nordam et al. (2019), Boufadel et al. (2020). See Supplementary Information for sensitivity analysis on the effect of choice of vertical diffusivity parametrization.

2.4. Individual-based model and toxicokinetics

Individuals are modelled as “biological particles” which are transported by ocean currents and experience growth and uptake and depuration of produced water components. In this section, we give a description of the parameters and processes that describe and affect the

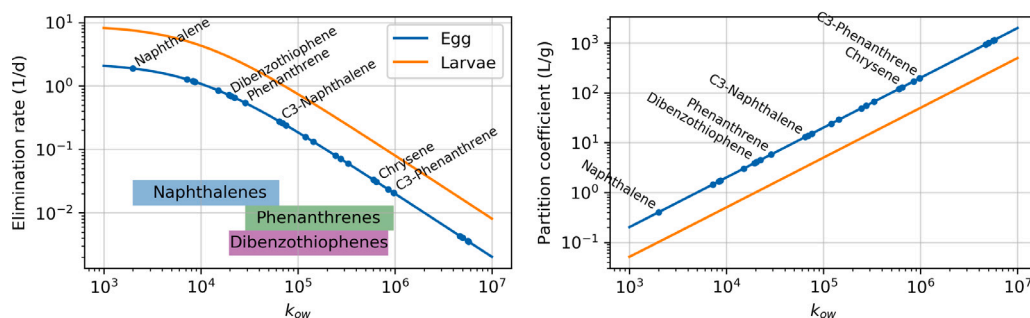


Fig. 3. Parameters values in the toxicokinetic model predicted by the OMEGA model, as a function of the octanol-water partition coefficient.

biological particles. Mathematical descriptions of the transport, growth and toxicokinetic models are given in the Supplementary Information, Eqs. 1 through 6. Each particle is a super-individual representing a fraction of a population and consisting of a collection of physically identical individuals (Scheffer et al., 1995). The super-individual has a state consisting of position, depth, stage, length, lipid content and internal concentrations. Particle positions are updated based on the local flow conditions and relevant inherent properties of the super-individual stage, such as buoyancy and vertical migration. In the present study we use a simplified model of the cod ELS with two distinct stages (eggs and larvae), corresponding to the two primary stages before the juvenile stage is reached (Kendall et al., 1981). Eggs are positively buoyant in seawater and are therefore found in the upper water masses. To represent this we use a constant rise speed of 0.2 mm/s, corresponding to a sphere of 0.7 mm in diameter and a density of 1 g/L below the ambient sea water density (see Sundby and Kristiansen, 2015). The egg stage is set to last for 10 days (100 degree-days at 10°C Fraser et al., 1988), and eggs have been given a lipid fraction of 20%, which is higher than typically reported for Atlantic cod eggs (see e.g. Finn et al., 1995). As such, the values of the corresponding partition coefficients in the toxicokinetic model are a high estimate for the egg stage. The egg stage is followed by a planktonic larval (and early juvenile stage) stage lasting for the remainder of the simulation (65 days), where a lower lipid fraction of 5% is used (see e.g. Li et al., 2015). The larval stage body length grows at a fixed rate of 0.05 day⁻¹, see von Bertalanffy growth model, Eq. 3 in the Supplementary Information. In reality this rate has a temperature dependence that we have not included here (see e.g. Otterlei et al., 1999). Vertical migration is not used for the larval stage, which has neutral buoyancy, and spread vertically due to turbulent diffusion. Other processes such as food limitation and natural mortality are not considered in the present study.

In this study, three known spawning grounds for Atlantic Cod were used (see e.g. Sundby et al., 2017), those with the closest proximity to clusters of produced water sources in the Norwegian part of the North Sea (Fig. 1). The spawning ground naming convention follows Akimova et al. (2019), with Viking Bank (VB) furthest north, Ling Bank (LB) in the middle and Fisher Bank (FB) furthest south. While the spawning season for cod covers several months (Sundby et al., 2017), we follow a one-day time-slice subset of the spawned eggs during a peak month (March 15th), which facilitates a clearer comparison of internal concentrations for the two distinct stages. A total of 30 000 super-individuals were used in the simulations, whose initial positions were randomly selected within the three spawning grounds at the day of spawning.

Depending on their three-dimensional position, super-individuals experience environmental concentrations of the different PW components from the concentration fields calculated by the fate model. From these concentrations the model calculates internal concentrations (or body residues) using a one-compartment toxicokinetic model (see e.g. Jager et al., 2011 and Supplementary Information Eq. 2), which also accounts for the effect of dilution by growth. In this type of model the individual organism is represented as a single well-mixed unit, where differences between internal and external (exposure)

concentrations drives the uptake and elimination (depuration) of PW components. The toxicokinetic equation is solved numerically for each super-individual and chemical component using a time step of 1 min.

There are two main parameters in the toxicokinetic model which governs the temporal changes of internal concentrations: the elimination rate (k_e , 1/day) and partition coefficient (P_{iw} , L/g). The elimination rate governs the transfer of PW components between the external environment and the organism, while the partition coefficient, also known as the bioconcentration factor, is the ratio of internal to external concentration at equilibrium. In addition to variation across species and life stages, these parameters are known to scale with the octanol-water partition coefficient (k_{ow}) for many substances, such as the PW components in the fate model considered here, and many functional relationships have been proposed (see e.g. French-McCay, 2002; Baas et al., 2015). Here we use the OMEGA model (Hendriks et al., 2001; De Hoop et al., 2013) to obtain parameter values for each PW component, which explicitly accounts for changes in the lipid fraction value (super-individual stage dependent) and body weight (superindividual age- and stage-dependent). The association between k_{ow} and parameter values is illustrated in Fig. 3 for the elimination rate (left panel) and partition coefficient (right panel), both for the egg and initial larvae stages. Note that as the larvae grow and their body masses increase, internal concentrations are reduced through dilution, and the elimination rate decreases (see Supplementary Information for further details).

2.5. Simulation scenarios

We have run simulations for four different years of currents (2009–2012), while all other model input and parameters were kept the same. The total simulation duration was 90 days, starting March 1st, and with continuous PW discharge. The first 15 days of the simulation were used as a “spin-up” period to establish external concentration fields, before egg spawning at day 14 (15th March). After 10 days in the egg stage, the individuals changed to the larval stage, which lasted for the remaining simulation duration (65 days).

3. Results

The produced water environmental concentrations tend to be highest near the point sources with the largest emissions, and most of these are found in the Tampen region (cf. Fig. 2). Consequently this is where the potential is highest for PW exposure to super-individuals, as seen in Fig. 4 from the areas indicating where concentration levels above 20 ng/L total PAH can occur (time- and depth-maximum). While these areas are largest around Tampen, smaller areas are also found around Utsira and Ekofisk. At the end of the simulations (all years), about 86% by mass of the total discharged PAHs has undergone primary biodegradation, while 0.1–0.5% or less has been advected outside the model domain.

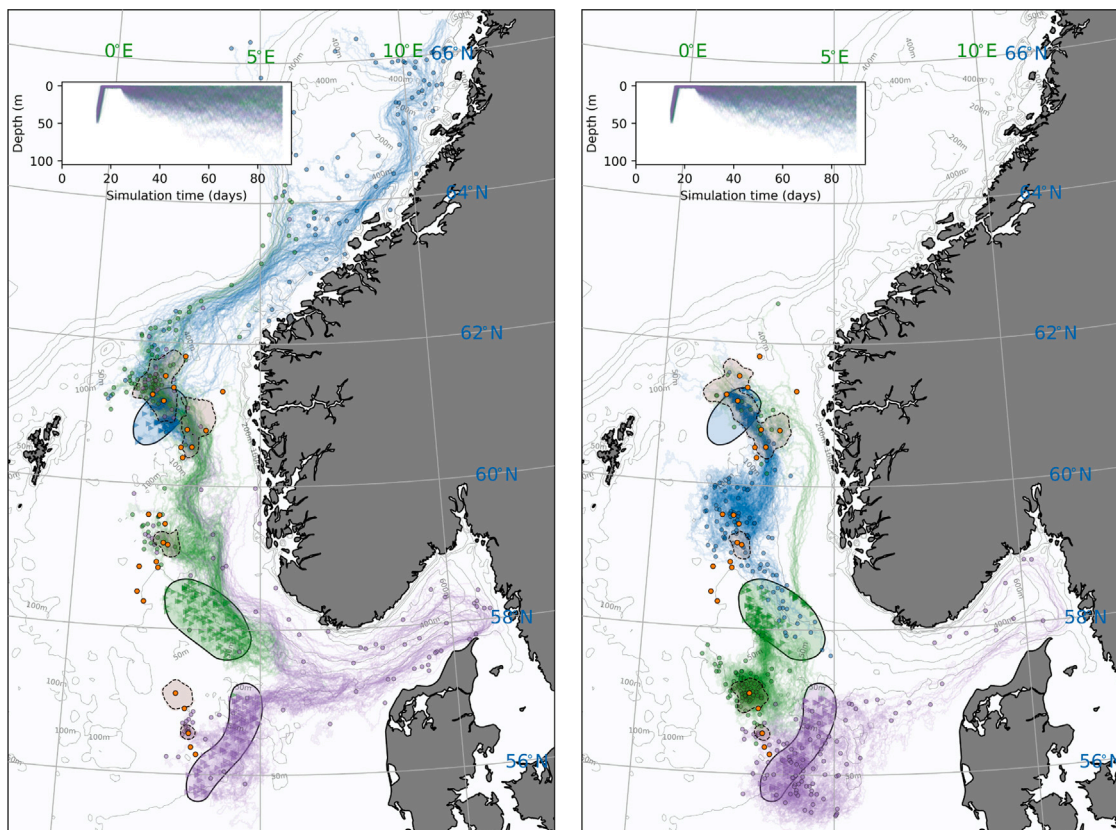


Fig. 4. Trajectories of the 100 super-individuals from each spawning ground with the highest total internal concentrations, 2010 simulation (left) and 2012 (right). Spawning grounds are indicated by the coloured polygons: purple (Fisher Bank), green (Ling Bank) and blue (Viking Bank). The trajectory colours indicate the originating spawning ground for each super-individual. Produced water discharge locations are shown as small orange circle markers. The shaded (light brown, dashed outline) areas around some of the discharge points show the area of maximum (over time and depth) dissolved total PAH concentrations exceeding 20 ng/L. The inset figure shows the depths of the super-individuals over time. (For interpretation of the references to colour in this figure legend, the reader is referred to the web version of this article.)

Following spawning, the super-individuals representing eggs are transported with currents, as shown in Fig. 4, where the colour coding indicates the spawning ground origin. For each spawning ground 100 individual trajectories are shown, corresponding to those super-individuals which incurred the highest total internal concentration. Based on the prevailing patterns in the circulation (Fig. 1), super-individuals from the same spawning ground have common patterns in their trajectories. From the southernmost spawning ground (Fisher Bank), most super-individuals are transported eastward, away from the platforms in the Ekofisk region, into the Skagerrak “loop” (Huserbråten et al., 2018), and end up in the Norwegian coastal current, being eventually transported northward. The super-individuals from the Ling Bank are transported northward, with some intersecting the Utsira High region. Finally, the Viking Bank super-individuals, starting out in the Tampen region, tend to follow northward trajectories, entraining into the North Atlantic current. This transport pattern is seen in the period 2009–2011. However, transport in 2012 is different, where there is a general advection of super-individuals in a south–southwest direction. In this year, super-individuals from VB end up in the Utsira High region, and super-individuals from LB end up in the Skagerrak loop, while there is little net transport from FB, and the end positions remain in the vicinity of the spawning ground. This can be seen in Fig. 4, where the left pane shows trajectories for 2010 as an example of the 2009 to 2011 years, and the right pane shows trajectories for 2012. Inset figures in Fig. 4 show the depth of bioparticles as a function of time. Vertical turbulent diffusivity is not high enough to overcome positive buoyancy in the egg stage, but causes gradual vertical mixing once the particles reach the larvae stage (see Supplementary Information for a sensitivity analysis of vertical diffusivity on model results).

In terms of uptake of PW components, we find that total internal PAH concentrations vary significantly between individuals, covering several orders of magnitude, both in the egg and larval stages. To quantify the overall population internal total PAH concentrations (26 components), we calculate summary statistics over all super-individuals, shown in Fig. 5. Statistical summary values for this figure may be found in Table 2 in the Supplementary Information. Here, the median and 95-percentile values (top and middle panel in Fig. 5) provide the total molar internal PAH concentration level below which 50% and 95% of the super-individuals fall, respectively. The highest inter-annual variability is found in the population-median value (upper panel), as indicated by the shaded region, covering one standard deviation from the simulations mean (over different years). We observe that the 95-percentiles (middle panel) attain maximum values at the end of the egg stage (around simulation day 25), for all years, and that the values are quite similar between years. Since the equilibrium value of internal concentrations, related to the partition coefficient P_{lw} , is higher for the egg stage than the larval stage due to differences in lipid fraction, it is plausible that just such a maximum can occur during the egg stage. Its position at the end of the stage following a continuous increase, when lipid fraction change in the super-individuals, further indicate that equilibrium was not reached. The figure also shows the maximum total internal PAH concentration reached among all super-individuals (lower panel), which in all scenarios is less than 1.24 nmol/g. These values are the highest observed over the entire population at any given time, and may originate from different super-individuals at different times. As such, they are more prone to random fluctuations (super-individual diffusive transport is a random process), and too much should not be read into the specific time development of the curves, but they do provide an upper bound on the observed internal concentration values.

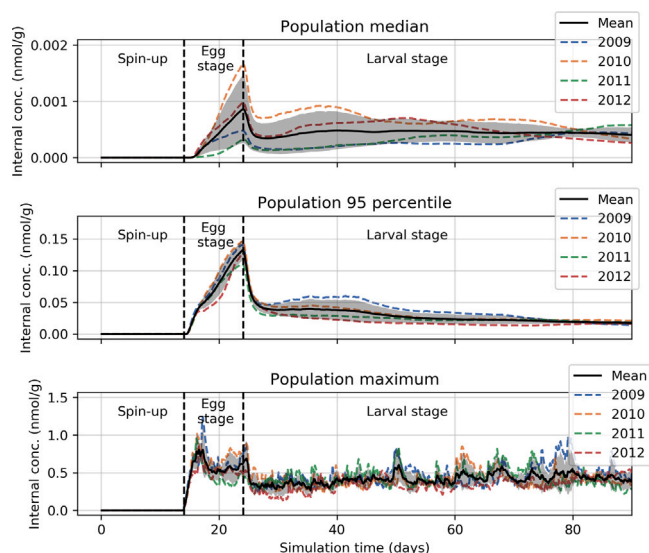


Fig. 5. Population total internal PAH concentration percentiles and maximum values over time, for different simulation years. The black lines are mean values taken over simulation years, while the shaded areas are \pm one standard deviation from that mean. The vertical black dashed lines delineate egg spawning start (leftmost line) and end of the egg stage (rightmost line) for the super-individuals. Top panel: population-median total internal PAH concentration. Middle panel: population 95-percentile total internal PAH concentration; 95% of super-individuals have a total internal concentration less than this. Lower panel: population-maximum total internal PAH concentration.

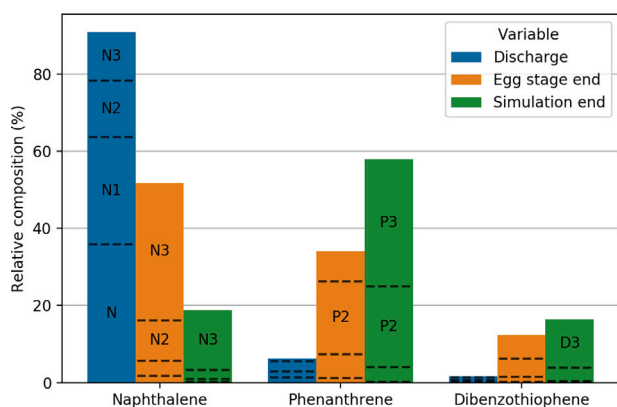


Fig. 6. Relative composition of the produced water discharge from all sources, compared with the relative composition of the total population internal PAH concentrations at two different times during the 2009 simulation. The relative compositions have been aggregated into three different component groups (see text). The individual components makeup is indicated by the dashed horizontal lines across the bars, and the larger of these have been labelled in shorthand (N: naphthalene, N1–N3: C1–C3 naphthalene, P2–P3: C2–C3 phenanthrene, D3: C3 dibenzothiophene).

The relative compositions of total internal PAH concentrations are shown in Fig. 6, summed into three different component groups, which combined make up more than 98% of the total internal concentrations. For reference, the total PAH discharge composition is shown, similarly grouped; also in this case the three groups constitute more than 98% the total. The numerical values for this figure may be found in Table 3 in the Supplementary Information. The relative composition of internal concentrations changes over time, with the naphthalenes group dominating at the end of the egg stage, while the phenanthrenes group is largest at the end of the simulation. For the dibenzothiophenes group, present in the discharge at only a few percent, a relative increase is seen in the internal concentration with simulation duration, ending up at 18% at the end. We note that naphthalene (the component, not the group) makes up 32% of the discharge, but is marginally present

in the internal concentrations ($< 1\%$), illustrating the importance of toxicokinetics, as well as biodegradation processes.

4. Discussion

A large part of the total produced water discharge undergoes bacterial degradation (biodegradation) in the simulations, with only 14% of the mass of the original components remaining after 90 days simulation time (not shown). Since biodegradation rates tend to decrease with increasing molecular size, smaller components such as naphthalene were rapidly degraded (see Supplementary Information Table 1 and Lofthuis et al., 2018). This makes the biodegradation process an important regulator of individual exposure concentrations. A biodegradable organic component will eventually turn into water and carbon dioxide through a degradation pathway that includes intermediate products. In this investigation the intermediate products are not explicitly tracked: primary (first step) degradation rates are used as input, and biodegraded masses are removed from the simulation, thus concentrations of intermediate degradation products are not considered. Heavier components (e.g. chrysene), which have lower biodegradation rates, will persist longer in the water column, and become more dominating in the exposure concentrations at greater distance from the discharge points. Conversely, the lighter components (e.g. naphthalene) occur mostly near the discharge points, due to their higher biodegradation rates.

In our simulations we released and followed spawning products from a single day. However, we expect that our conclusions will hold also for other dates within the peak spawning period, since the period large-scale transport patterns are broadly similar, and the PW discharge rates are constant. We also find that inter-year variability in the population internal concentration statistics is not very large. While the transport patterns for the 2009–2011 simulations are similar, the 2012 simulation has a markedly different pattern (Fig. 4), but this difference is not reflected in the general population internal concentrations 95-percentile (middle panel) and maximum values (lower panel) shown in Fig. 5. The population-median (upper panel) does show more variability, with a difference of almost an order of magnitude between highest and lowest at the end of the egg stage. It may be that since there are large single emission sources in each of the regions, similar internal concentrations levels can result from different transport pathways as PW plumes and spawning products are transported together. We note here that the super-individuals with the highest internal concentrations at the end of the simulation are not concentrated in a small region, but rather spread out (see Fig. 4). In terms of originating spawning ground, it is the sub-population from VB (Tampen area, blue in Fig. 4) that have the highest internal concentration (data not shown), which perhaps not surprising due to the greater number of high volume PW discharge sources in this area, and partial overlap of these with the spawning ground.

Previous studies of produced water discharges in the North Sea have found that environmental risks associated with these discharges are largely local, restricted to the immediate vicinity of the emission source (see e.g. Hylland et al., 2008; Brooks et al., 2011; Durell et al., 2006; Bakke et al., 2013). In a model study focusing on the alkylphenol components of produced water, Beyer et al. (2012) found that the environmental exposure concentration and internal concentrations ($C_4 - C_5$ and C_{6+} components) were too low to have an impact on the reproductive health of three different species of fish. From the bi-annual monitoring program conducted on the NCS, total internal PAH concentration in caged blue mussels placed near a produce water discharge (Tampen region) was in one study found to be up to 205 ng/g (w.w.) (Durell et al., 2006). A more recent iteration of the program included copepod sampling in the Tampen area, and found a mean total internal PAH concentration of 231 ± 102 ng/g (w.w.) (Hansen et al., 2020). The present simulations show a maximum value of 198 ng/g (1.2 nmol/g), and the 95-percentile values are all below 27 ng/g (0.15 nmol/g). Due to the difference in species (mussels, copepods,

cod), physiology (size, development stage, lipid content, etc.), as well as exposure dynamics (fixed cages, pelagic drift, vertical migration), these values are not directly comparable; qualitatively, however, it is useful to know where the model-predicted internal concentrations place themselves relative to field measurements.

In the present study, we may compare the total internal PAH concentrations, expressed in molar units (e.g. nmol/g), with known thresholds for adverse effects. For non-polar organic compounds, such as the PAHs considered here, the effect threshold for general acute narcosis is in the range 2–8 $\mu\text{mol/g}$ (wet weight) (Meador et al., 2011), which is three orders of magnitude above the highest levels seen in the present simulations. Sub-lethal effects are less readily assessed with this simplified approach, but if we apply an acute-to-chronic ratio (ACR) of 1000 (Ahlers et al., 2006), the levels remain below the threshold. The actual ACR is likely lower, in the 1–100 range, see e.g. Mcgrath et al. (2018) and Scholz et al. (2018). We must stress that only the measured PAH subset of components in the produced water discharges are considered here, and that other components would also contribute towards the total internal concentration levels, and must thus be considered when making conclusions regarding overall effects. Similarly, intermediate microbial biodegradation products of the primary components have not been included, and these may also contribute to body burden and toxicity (Hansen et al., 2018). The significance of such components would depend on their concentration in the discharge, environmental fate properties, and on toxicokinetics properties, as we have illustrated here for specific PAHs. Even at the embryonic stage, cold-water marine fish are able to produce biotransformation enzymes (Sørhus et al., 2016) which can metabolize heavy PAHs, causing alterations of the total PAH internal concentrations over time (Sørensen et al., 2017). This process is not accounted for in the present simulations.

5. Conclusion

We have developed a toxicokinetic-individual-based model coupled to an existing transport and fate model (DREAM), and used it to study uptake of polycyclic aromatic hydrocarbons from produced water sources in the North Sea (Norwegian side) in early life stages of Atlantic cod. The highest levels of total internal PAH concentration we find are 1.2 nmol/g (198 ng/g), with 95-percentiles generally below 0.15 nmol/g (27 ng/g), which are below thresholds that are expected to cause chronic effects. Inter-annual variations are found in the transport patterns of the eggs and larvae, but the population-level internal concentrations remain similar between the years. A large variation in relative composition of internal concentrations compared to discharges are found, demonstrating the importance of toxicokinetic models and their usefulness as a building block in assessment of environmental effects and risk.

CRedit authorship contribution statement

Raymond Nepstad: Conceptualization, Methodology, Software, Investigation, Data curation, Writing - original draft, Writing - review & editing, Visualization, Project administration, Funding acquisition. **Bjørn Henrik Hansen:** Conceptualization, Writing - original draft, Writing - review & editing. **Jørgen Skancke:** Conceptualization, Data curation, Writing - original draft, Writing - review & editing.

Declaration of competing interest

The authors declare that they have no known competing financial interests or personal relationships that could have appeared to influence the work reported in this paper.

Acknowledgements

The authors are grateful to Eirin Sva Stomperudhaugen at Miljødirektoratet (Norwegian Environment Agency) for providing the produced water discharge data. This work was performed as a part of the Joint Industry Project *DREAM-MER Phase II*, funded by Aker BP, Norway, Equinor, Norway, NOROG, Norway, Total E&P Norge, Norway and Vår Energi, Norway.

Appendix A. Supplementary data

Supplementary material related to this article can be found online at <https://doi.org/10.1016/j.marenvres.2020.105203>.

References

- Ahlers, J., Riedhammer, C., Vogliano, M., Ebert, R.U., Kühne, R., Schüürmann, G., 2006. Acute to chronic ratios in aquatic toxicity—variation across trophic levels and relationship with chemical structure. *Environ. Toxicol. Chem. SETAC* 25 (11), 2937–2945.
- Akimova, A., Hufnagl, M., Peck, M.A., 2019. Spatiotemporal dynamics of predators and survival of marine fish early life stages: Atlantic cod (*Gadus morhua*) in the North Sea. *Prog. Oceanogr.* 176 (August 2018), 102121.
- Alver, M.O., Broch, O.J., Melle, W., Bagoien, E., Slagstad, D., 2016. Validation of an Eulerian population model for the marine copepod *Calanus finmarchicus* in the Norwegian Sea. *J. Mar. Syst.* 160, 81–93.
- Ashauer, R., Escher, B.I., 2010. Advantages of toxicokinetic and toxicodynamic modelling in aquatic ecotoxicology and risk assessment. *J. Environ. Monitor.* 12 (11), 2056–2061.
- Baas, J., Spurgeon, D., Broerse, M., 2015. A simple mechanistic model to interpret the effects of narcotics. *SAR QSAR Environ. Res.* 26 (3), 165–180.
- Bagi, A., Pampanin, D.M., Brakstad, O.G., Kommedal, R., 2013. Estimation of hydrocarbon biodegradation rates in marine environments: A critical review of the Q10 approach. *Mar. Environ. Res.* 89, 83–90.
- Bakke, T., Klungsoyr, J., Sanni, S., 2013. Environmental impacts of produced water and drilling waste discharges from the Norwegian offshore petroleum industry. *Mar. Environ. Res.* 92, 154–169.
- Berenshtein, I., Paris, C.B., Perlin, N., Alloy, M.M., Joye, S.B., Murawski, S., 2020. Invisible oil beyond the Deepwater Horizon satellite footprint. *Sci. Adv.* 6 (7), 1–12.
- Beyer, J., Goksøyr, A., Hjermmann, D.Ø., Klungsoyr, J., 2020. Environmental effects of offshore produced water discharges: A review focused on the Norwegian continental shelf. *Mar. Environ. Res.* 162, 105155.
- Beyer, J., Myhre, L.P., Sundt, R.C., Meier, S., Tollefsen, K.E., Vabø, R., Klungsoyr, J., Sanni, S., 2012. Environmental risk assessment of alkylphenols from offshore produced water on fish reproduction. *Mar. Environ. Res.* 75, 2–9.
- Boufadel, M.C., Abdollahi-Nasab, A., Geng, X., Galt, J., Torlapati, J., 2014. Simulation of the landfall of the deepwater horizon oil on the shorelines of the Gulf of Mexico. *Environ. Sci. Technol.* 48 (16), 9496–9505.
- Boufadel, M., Liu, R., Zhao, L., Lu, Y., Özgökmen, T., Nedwed, T., Lee, K., 2020. Transport of oil droplets in the upper ocean: Impact of the eddy diffusivity. *J. Geophys. Res. Oceans* 125 (2), e2019JC015727.
- Brander, K., 2005. Spawning and Life History Information for North Atlantic Cod Stocks. Technical Report 274.
- Brooks, S.J., Harman, C., Grung, M., Farmen, E., Ruus, A., Vingen, S., Godal, B.F., Baršienė, J., Andreikenaitė, L., Skarphéinsdóttir, H., Liewenborg, B., Sundt, R.C., 2011. Water column monitoring of the biological effects of produced water from the ekofisk offshore oil installation from 2006 to 2009. *J. Toxicol. Environ. Health A: Curr. Issues* 74 (7–9), 582–604.
- De Hoop, L., Huijbregts, M.A.J., Schipper, A.M., Veltman, K., De Laender, F., Viaene, K.P.J., Klok, C., Hendriks, A.J., Hoop, L.D., De, F., 2013. Modelling bioaccumulation of oil constituents in aquatic species. *Mar. Pollut. Bull.* 76 (1–2), 178–186.
- Durell, G., Frost, T., Neff, J., 2006. Oil well produced water discharges to the North Sea. Part I: Comparison of deployed mussels (*Mytilus edulis*), semi-permeable membrane devices, and the DREAM model predictions to estimate the dispersion of polycyclic aromatic hydrocarbons. *Mar. Environ. Res.* 62, 194–223.
- Equinor, 2018. Årsrapport 2018 for Gullfaksfeltet. Technical Report, Equinor.
- Faksness, L.-G., Grini, P.G., Daling, P.S., 2004. Partitioning of semi-soluble organic compounds between the water phase and oil droplets in produced water. *Mar. Pollut. Bull.* 48 (7–8), 731–742.
- Finn, R., Henderson, J., Fyhn, H., 1995. Physiological energetics of developing embryos and yolk-sac larvae of Atlantic cod (*Gadus morhua*). II. Lipid metabolism and enthalpy balance. *Mar. Biol.* 124 (3), 371–379.
- Fraser, A.J., Gamble, J.C., Sargent, J.R., 1988. Changes in lipid content, lipid class composition and fatty acid composition of developing eggs and unfed larvae of cod (*Gadus morhua*). *Mar. Biol.* 99 (3), 307–313.

- French-McCay, D.P., 2002. Development and application of an oil toxicity and exposure model, OilToxEx. *Environ. Toxicol. Chem. SETAC* 21 (10), 2080–2094.
- Grimm, V., Railsback, S.F., 2005. *Individual-based Modeling and Ecology*. Princeton University Press, New Jersey, p. 428.
- Hansen, B.H., Farkas, J., Nordtug, T., Altin, D., Brakstad, O.G., 2018. Does microbial biodegradation of water-soluble components of oil reduce the toxicity to early life stages of fish? *Environ. Sci. Technol.* 52 (7), 4358–4366.
- Hansen, B.H., Sørensen, L., Størseth, T.R., Altin, D., Gonzalez, S.V., Skancke, J., Rønsberg, M.U., Nordtug, T., 2020. The use of PAH, metabolite and lipid profiling to assess exposure and effects of produced water discharges on pelagic copepods. *Sci. Total Environ.* 714, 136674.
- Hansen, B.H., Sørensen, L., Størseth, T.R., Nepstad, R., Altin, D., Krause, D., Meier, S., Nordtug, T., 2019. Embryonic exposure to produced water can cause cardiac toxicity and deformations in Atlantic cod (*Gadus morhua*) and haddock (*Melanogrammus aeglefinus*) larvae. *Mar. Environ. Res.* 148 (May), 81–86.
- Hendriks, A., van der Linde, A., Cornelissen, G., Sijm, D., 2001. The power of size. 1. Rate constants and equilibrium ratios for accumulation of organic substances related to octanol-water partition ratio and species weight. *Environ. Toxicol. Chem. SETAC* 20 (7), 1399–1420.
- Huserbråten, M.B., Moland, E., Albreten, J., 2018. Cod at drift in the North Sea. *Prog. Oceanogr.* 167, 116–124.
- Hylland, K., Tollefsen, K.E., Ruus, A., Jonsson, G., Sundt, R.C., Sanni, S., Røe Utvik, T.I., Johnsen, S., Nilsen, I., Pinturier, L., Balk, L., Baršienė, J., Marigómez, I., Feist, S.W., Børseth, J.F., 2008. Water column monitoring near oil installations in the North Sea 2001–2004. *Mar. Pollut. Bull.* 56 (3), 414–429.
- Jager, T., Albert, C., Preuss, T.G., Ashauer, R., 2011. General unified threshold model of survival - A toxicokinetic-toxicodynamic framework for ecotoxicology. *Environ. Sci. Technol.* 45 (7), 2529–2540.
- Kendall, A., Ahlstrom, E., Moser, H., 1981. Early life history stages of fishes and their characters. In: *Ontogeny and Systematics of Fishes*. pp. 1–12.
- Li, K., Østensen, M.A., Attramadal, K., Winge, P., Sparstad, T., Bones, A.M., Vadstein, O., Kjorsvik, E., Olsen, Y., 2015. Gene regulation of lipid and phospholipid metabolism in Atlantic cod (*Gadus morhua*) larvae. *Comp. Biochem. Physiol. B Biochem. Mol. Biol.* 190, 16–26.
- Lofthus, S., Almås, I.K., Evans, P., Pelz, O., Brakstad, O.G., 2018. Biodegradation in seawater of PAH and alkylphenols from produced water of a North Sea platform. *Chemosphere* 206, 465–473.
- McCarty, L.S., Mackay, D., 1993. Enhancing ecotoxicological modeling and assessment. Body residues and modes of toxic action. *Environ. Sci. Technol.* 27 (9), 1718–1728.
- Mcgrath, J.A., Fanelli, C.J., Di Toro, D.M., Parkerton, T.F., Redman, A.D., Paumen, M.L., Comber, M., Eadsforth, C.V., den Haan, K., 2018. Re-evaluation of target lipid model-derived HC5 predictions for hydrocarbons. *Environ. Toxicol. Chem.* 9999 (9999), 1–15.
- Meador, J.P., Adams, W.J., Escher, B.I., McCarty, L.S., McElroy, A.E., Sappingtony, K.G., 2011. The tissue residue approach for toxicity assessment: Findings and critical reviews from a society of environmental toxicology and chemistry pelston workshop. *Integr. Environ. Assess. Manage.* 7 (1), 2–6.
- Meador, J.P., McCarty, L.S., Escher, B.I., Adams, W.J., 2008. 10th anniversary critical review: The tissue-residue approach for toxicity assessment: concepts, issues, application, and recommendations. *JEM* 10, 1486–1498.
- Neff, J., Lee, K., DeBlois, E.M., 2011. Produced water: overview of composition, fates, and effects. In: *Produced Water*. Springer, pp. 3–54.
- Niu, H., Lee, K., Robinson, B., Cobanli, S., Li, P., 2016. Monitoring and modeling the dispersion of produced water on the Scotian Shelf. *Environ. Syst. Res.* 5 (1), 19.
- Nordam, T., Beegle Krause, C.J., Skancke, J., Nepstad, R., Reed, M., 2019. Improving oil spill trajectory modelling in the Arctic. *Mar. Pollut. Bull.* 140 (January), 65–74.
- NOROG, 2018. Miljørapport 2018. Technical Report, Norsk olje og gass.
- Otterå, H., 2004. FAO cultured aquatic species information programme - *Gadus morhua*. In: *Cultured Aquatic Species Information Programme*. FAO Fisheries and Aquaculture Department.
- Otterlei, E., Nyhammer, G., Folkvord, A., Stefansson, S.O., 1999. Temperature- and size-dependent growth of larval and early juvenile Atlantic cod (*Gadus morhua*): a comparative study of Norwegian coastal cod and northeast Arctic cod. *Can. J. Fish. Aquat. Sci.* 56 (11), 2099–2111.
- Paris, C.B., Hénaff, M.L., Aman, Z.M., Subramaniam, A., Helgers, J., Wang, D.P., Kourafalou, V.H., Srinivasan, A., 2012. Evolution of the Macondo well blowout: Simulating the effects of the circulation and synthetic dispersants on the subsea oil transport. *Environ. Sci. Technol.* 46 (24), 13293–13302.
- Reed, M., Hetland, B., 2002. DREAM: a dose-related exposure assessment model technical description of physical-chemical fates components. In: *Proceedings of SPE International Conference on Health, Safety and Environment in Oil and Gas Exploration and Production*. Society of Petroleum Engineers.
- Reed, M., Rye, H., 2011. The DREAM model and the environmental impact factor: Decision support for environmental risk management. In: *Produced Water*. Springer, pp. 189–203.
- Scheffer, M., Baveco, J.M., DeAngelis, D.L., Rose, K.A., van Nes, E.H., 1995. Super-individuals a simple solution for modelling large populations on an individual basis. *Ecol. Model.* 80 (2–3), 161–170.
- Scholz, S., Schreiber, R., Armitage, J., Mayer, P., Escher, B.I., Lidzba, A., Léonard, M., Altenburger, R., 2018. Meta-analysis of fish early life stage tests - Association of toxic ratios and acute-to-chronic ratios with modes of action. *Environ. Toxicol. Chem.* 37 (4), 955–969.
- Simonsen, M., Saetra, Ø., Isachsen, P.E., Lind, O.C., Skjerdal, H.K., Salbu, B., Helledal, H.E., Gwynn, J.P., 2017. The impact of tidal and mesoscale eddy advection on the long term dispersion of 99Tc from Sellafield. *J. Environ. Radioact.* 177, 100–112.
- Slagstad, D., McClimans, T., 2005. Modeling the ecosystem dynamics of the Barents sea including the marginal ice zone: I. Physical and chemical oceanography. *J. Mar. Syst.* 58 (1–2), 1–18.
- Smagorinsky, J., 1963. General circulation experiments with the primitive equations. *Mon. Weather Rev.* 91 (3), 99–164.
- Smit, M.G., Frost, T.K., Johnsen, S., 2011. Achievements of risk-based produced water management on the Norwegian continental shelf (2002–2008). *Integr. Environ. Assess. Manage.* 7 (4), 668–677.
- Sørensen, L., Hansen, B.H., Farkas, J., Donald, C., Robson, W., Tonkin, A., Meier, S., Rowland, S.J., 2019. Accumulation and toxicity of monoaromatic petroleum hydrocarbons in early life stages of cod and haddock.
- Sørensen, L., Sørhus, E., Nordtug, T., Incardona, J.P., Linbo, T.L., Giovanetti, L., Karlsen, Ø., Meier, S., 2017. Oil droplet fouling and differential toxicokinetics of polycyclic aromatic hydrocarbons in embryos of Atlantic haddock and cod. *PLoS One* 12 (7), 1–26.
- Sørhus, E., Incardona, J.P., Karlsen, Ø., Linbo, T., Sørensen, L., Nordtug, T., Van Der Meeren, T., Thorsen, A., Thorbjørnsen, M., Jentoft, S., Edvardsen, R.B., Meier, S., 2016. Crude oil exposures reveal roles for intracellular calcium cycling in haddock craniofacial and cardiac development. *Sci. Rep.* 6 (5020), 1–21.
- Sundby, S., Kristiansen, T., 2015. The principles of buoyancy in Marine Fish Eggs and their vertical distributions across the World Oceans. *PLoS One* 10 (10), 1–23.
- Sundby, S., Kristiansen, T., Nash, R.D., Johannesen, T., 2017. Dynamic mapping of north sea spawning: Report of the KINO project. In: *Fisken Og Havet, Vol. 2*. Technical Report 2, p. 183.
- Vikebø, F., Jørgensen, C., Kristiansen, T., Fiksen, Ø., 2007. Drift, growth, and survival of larval Northeast Arctic cod with simple rules of behaviour. 347, 207–219.